marine drugs

MDPI

Article

Novel Discorhabdin Derivatives from Antarctic Sponges of the Genus *Latrunculia*: Expanding the Chemical Diversity of Polar Marine Natural Products

Sam Afoullouss [1,†], Stine S. H. Olsen [1,†], Sydney Morrow [1], Ezequiel Cruz Rosa [1], Kaley Geu [1], Nerida G. Wilson [2,3] and Bill J. Baker [1,*]

[1] Department of Chemistry, University of South Florida, 4202 E. Fowler Avenue, CHE205, Tampa, FL 33620, USA; samafoullouss@usf.edu (S.A.); olsens@usf.edu (S.S.H.O.); kalyn12@usf.edu (S.M.); ecruzrosa@usf.edu (E.C.R.); geuk@usf.edu (K.G.)
[2] School of Biological Sciences, The University of Western Australia, 35 Stirling Highway, Crawley, WA 6009, Australia; nerida.wilson@uwa.edu.au
[3] Collections & Research, Western Australian Museum, 49 Kew Street, Welshpool, WA 6106, Australia
* Correspondence: bjbaker@usf.edu
† These authors contributed equally to this work.

Abstract

In this study, three Antarctic sponges of the genus *Latrunculia* were investigated, leading to the isolation of five unreported pyrroloiminoquinone alkaloids along with the known metabolite (+)-debromodiscorhabdin A (**3**). Three of the new metabolites were brominated, while the other two were found to have a C-5/C-8 sulfur bridge and a C-2/N-18 bridge. Three of the metabolites were shown to have a phenyl ketone substituent on C-14, not previously reported for discorhabdin derivatives. The cytotoxicity against the A549 cell lines was studied and compounds **1**–**4** showed activity of 4.3, 1.8, 1.0, and 23.9 μM, respectively, while no inhibition was found for **5** and **6**.

Keywords: Discorhabdin; DFT; ECD; Antarctic; sponge

Academic Editor: Manolis Mandalakis

Received: 7 August 2025
Revised: 7 October 2025
Accepted: 8 October 2025
Published: 15 October 2025

Citation: Afoullouss, S.; Olsen, S.S.H.; Morrow, S.; Cruz Rosa, E.; Geu, K.; Wilson, N.G.; Baker, B.J. Novel Discorhabdin Derivatives from Antarctic Sponges of the Genus *Latrunculia*: Expanding the Chemical Diversity of Polar Marine Natural Products. *Mar. Drugs* **2025**, *23*, 401. https://doi.org/10.3390/md23100401

1. Introduction

Sponges of the genus *Latrunculia* (family: Latrunculiidae; class: Demospongiae) are known for producing cytotoxic pyrroloiminoquinone alkaloids known as discorhabdins, a name derived from the unusual discorhabd spicules that characterize the sponge family [1,2]. The sponges are commonly found in cold habitats, mainly Antarctica and the North Pacific [3]. They are known to produce a significant variety of secondary metabolites, but mainly the highly pigmented discorhabdins, many of which have shown strong activity against various cancer cell lines [4]. Discorhabdins described to date consist of a pentacyclic backbone of 18 carbons and 3 nitrogen atoms with a C-6 spiro-center and a C-11 ketone, or di- and trimers thereof [5,6]. The backbone displays various substitution including mono- and dibromination and a C-5/C-8 sulfur bridge [5].

The research discussed herein involves the investigation of three specimens of the genus *Latrunculia* sp. collected in Antarctica at two different locations. During a circumpolar cruise of Antarctica, led by the Swiss Polar Institute in 2016, two specimens of *Latrunculia* cf. *biformis* were obtained by trawl from the Kerguelen Plateau. A third, as yet unidentified, specimen of *Latrunculia* sp. was collected by SCUBA from the Palmer Archipelago in 2018. The metabolites were prioritized based on an MS-guided fractionation by pursuing

fractions with a 1:1 or 1:2:1 isotopic pattern, indicative of mono- and dibrominated metabolites, combined with targeting aromatic ^{1}H NMR signals. Five new metabolites with the discorhabdin backbone, illustrated in Figure 1, were isolated and characterized and one known metabolite, (+)-debromodiscorhabdin A (**3**), was identified through a comparison of its spectroscopic data to that previously published [7]. The metabolites were characterized through 1D/2D Nuclear Magnetic Resonance (NMR) Spectroscopy data, high-resolution mass spectrometry (HR-MS), and comparison of experimental and calculated chemical shifts, using DP4+ and Sorted Training Set (STS) comparison tools, and Electronic Circular Dichroism (ECD) spectra.

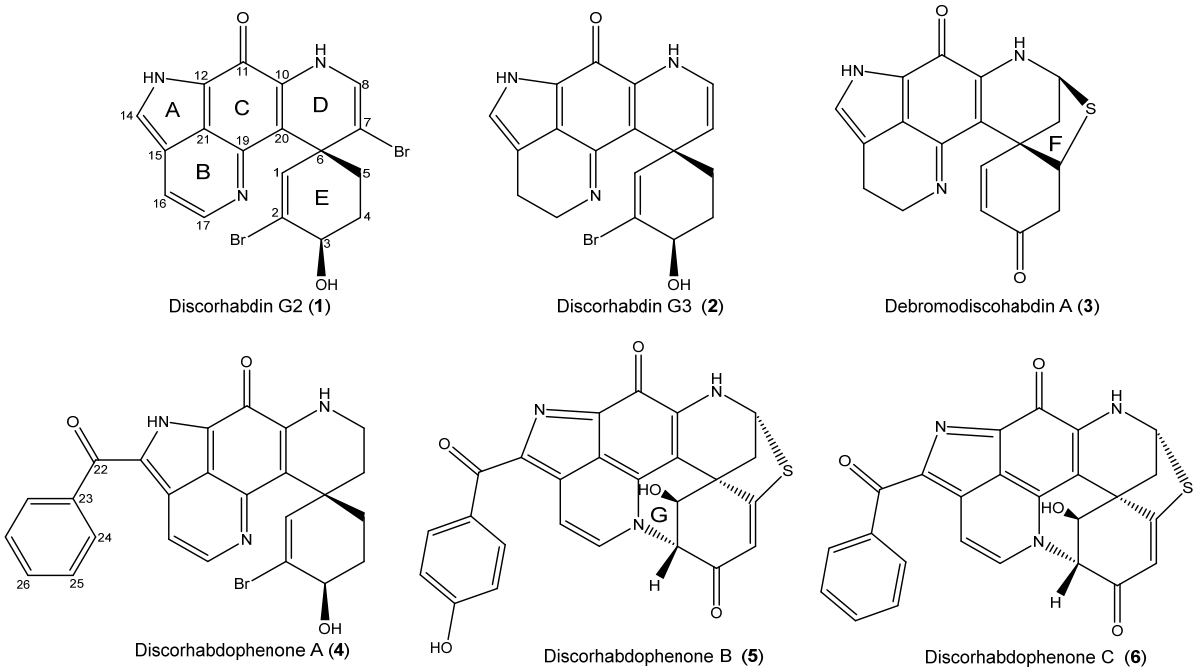

Figure 1. Alkaloids isolated from Antarctic sponges *Latrunculia* cf. *biformis* and *Latrunculia* sp.

2. Results and Discussion

2.1. Structure Elucidation

Discorhabdin G2 (7-bromo-3-dihydro-16,17-dehydrodiscorhabdin G, **1**) was obtained from the 50% MeOH/H_2O eluent from the *Latrunculia* cf. *biformis* specimen designated ACE16-49 (WAMZ44145). It was isolated as a deep-red solid with the pseudo-molecular ion peak at *m*/*z* 463.9450 ([M + H]$^+$, HRESIMS) and a 1:2:1 isotopic pattern, indicative of two bromine atoms in the molecule. The ^{1}H and ^{13}C NMR data (Table 1) corroborated the molecular formula as $C_{18}H_{13}Br_2N_3O_2$. The 18 carbon and 3 nitrogen atoms indicated that the compound had the backbone of the discorhabdins. The NMR data suggested that **1** had five olefinic protons; ten quaternary carbons, with nine of these being deshielded; one oxymethine; and two methylene groups.

The structure was elucidated starting from homonuclear correlation spectroscopy (COSY) and Heteronuclear Multiple Bond Correlation (HMBC) correlations, as illustrated in Figure 2. Key correlations include COSY correlation between the oxymethine H-3 (δ_H 4.42) and H_2-4 (δ_H 2.18/2.04) and further to H_2-5 (δ_H 2.70/2.11). HMBC correlations were displayed from H-3 to the olefinic proton C-1 (δ_C 134.9) and quaternary carbon C-2 (δ_C 129.2). H-1 (δ_H 6.15) had HMBC correlations to C-2, C-3 (δ_C 67.3), C-5 (δ_C 36.9), C-6 (δ_C 45.9), C-7 (δ_C 104.0), and C-20 (δ_C 111.7). H_2-4 and H_2-5 showed HMBC correlations to C-3 and C-6, while H_2-5 also showed correlations to C-7 and C-20. The high-field quaternary carbon C-6 was indicative of the spiro-center between rings D and E of the discorhabdin

backbone, with C-3 often displaying an oxymethine. The H-8 (δ_H 6.60) olefinic proton had COSY correlation to the H-9 (δ_H 8.72) exchangeable proton and HMBC correlations to quaternary carbons C-6, C-7, and C-10 (δ_C 137.9), establishing the Δ^7-olefin. Further HMBC correlations between H-9 and C-20 completed the assignment of the D and E rings of a discorhabdin skeleton, and another correlation to C-11 (δ_C 164.1) extended that ring system to the iminoquinone ketone.

Table 1. NMR data for Discorhabdin G2 and Discorhabdin G3 (**1** and **2**) (600 (^{1}H) and 150 (^{13}C) MHz, $(CD_3)_2SO$)).

Pos.	1				2	
	δ_C, Type	**δ_H (*J* in Hz)**	**gCOSY**	**gHMBC**	**δ_C, Type**	**δ_H (*J* in Hz)**
1	134.9, CH	6.15, s		2, 3, 5, 6, 7, 20	134.7, CH	6.33, s
2	129.2, C				132.1, C	
3	67.3, CH	4.42, t (7.1)	4a, 4b	1, 2, 4	67.2, CH	4.42, t (7.8)
4a	32.7, CH_2	2.18, qt (13.1, 4.4)	3, 4b, 5a	2, 3, 5, 6	27.4, CH_2	1.91, dt (7.3, 3.0)
4b		2.04, dq (4.9, 7.5)	3, 4a	2, 3, 5, 6		
5a	36.9, CH_2	2.70, td (13.6, 4.0)	4a, 5b	3, 4, 6, 7, 20	34.9, CH_2	2.27, m
5b		2.11, dt (14.0, 3.6)		1, 3, 4, 6, 7, 20		1.84, d (13.1)
6	45.9, C				40.3, C	
7	104.0, C				115.4, CH	5.24, d (7.6)
8	125.5, CH	6.60, d (5.3)	9	6, 7, 10	121.8, CH	6.28, dd (3.1, 4.5)
9		8.72, d (4.2)	8	7, 11, 20		10.43, s
10	137.9, C				144.6, C	
11	164.1, C				166.4, C	
12	118.5, C				123.4, C	
13						13.17, s
14	128.6, CH	8.24, s		11, 12, 15, 21	126.8, CH	7.36, s
15	124.6, C				119.4, C	
16	113.7, CH	7.54, d (5.8)	17	14, 17, 19, 21	17.9, CH_2	2.87, t (7.5)
17	141.6, CH	8.31, d (5.8)	16	15, 16, 19, 21	44.8, CH_2	3.91, dd (5.9, 7.1)
18						8.78, s
19	147.3, C				157.2, C	
20	111.7, C				99.6, C	
21	119.5, C				122.4, C	

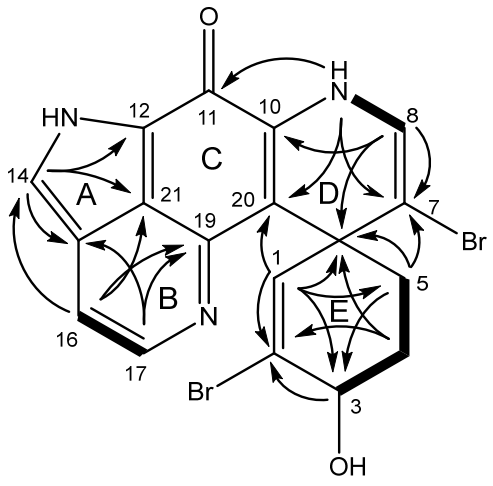

Figure 2. COSY (bold) and HMBC (arrow) correlations of **1**.

The olefinic protons H-16 (δ_H 7.54) and H-17 (δ_H 8.31) showed COSY correlation to each other, while H-16 showed HMBC correlations to C-14 (δ_C 128.6), C-17 (δ_C 141.6), C-19

(δ_C 147.3), and C-21 (δ_C 119.5) and H-17 showed HMBC correlations to C-15 (δ_C 124.6), C-16 (δ_C 113.7), C-19, and C-21. This suggested that the olefin was on ring B. The remaining olefinic proton (H-14, δ_H 8.24) had HMBC correlations to quaternary carbons C-11 (δ_C 164.1), C-12 (δ_C 118.5), C-15, and C-21. Correlation from H-9 and H-14 on opposite sides of the molecule to C-11, indicated this deshielded quaternary carbon to be the carbonyl displayed in the discorhabdin backbone on ring C. The two bromines indicated by the HRESIMS were placed on the two open valences C-2 and C-7, completing the planar structure of **1**.

Discorhabdin G3 (3-dihydrodiscorhabdin G, **2**) was obtained from the same extract as **1** and was isolated as a green solid with the molecular formula $C_{18}H_{16}BrN_3O_2$, corroborated by the *m*/*z* of 386.0505 (HRESIMS, $[M + H]^+$) and its ^1H and ^{13}C NMR data. The molecular formula indicated **2** to have three extra protons and one fewer bromine compared to **1**, while its ^1H NMR spectrum suggested **2** to have two of the olefinic protons replaced by methylene groups. The 2D NMR data (Table S2) suggested the two compounds to display significant similarities, with the only differences being a lack of bromine at C-7 and reduction in the Δ^{16}-olefin. The missing bromine was replaced by a new methine at δ_H 5.24 (H-7) with COSY correlation to H-8 (δ_H 6.28). The reduction in the Δ^{16}-olefin was established by COSY correlation between the methylene protons H_2-16 (δ_H 2.87) and H_2-17 (δ_H 3.91) and HMBC correlations to C-14 (δ_C 126.8), C-15 (δ_C 119.4), C-17 (δ_C 44.8), C-21 (δ_C 122.4), and C-16 (δ_C 17.9) and C-19 (δ_C 157.2), respectively.

The 1D and 2D NMR data for **2** had significant similarities to the published data for discorhabdin G, published in 1995 by Yang et al. from *Latrunculia apicalis,* collected from the vicinity of McMurdo station in Antarctica [8]. Discorhabdin G was published with a molecular formula of $C_{18}H_{15}BrN_3O_2$, suggesting the loss of two protons compared to **2**. This matched the suggested structure elucidation with the C-3 ketone for discorhabdin G undergoing a reduction to the C-3 hydroxyl found for **2**.

A second specimen of *Latrunculia* cf. *biformis* from the 2016 sampling campaign, designated ACE16-51 (WAMZ144147), also produced two pyrroloiminoquinone metabolites, one of which was the known *Latrunculia*-derived metabolite debromodiscorhabdin A (**3**) based on comparison of NMR (Table S3) and mass spectral data to published values. Discorhabdophenone A (**4**) was isolated as a deep-red solid with a formula of $C_{25}H_{20}BrN_3O_3$, corroborated by ^1H and ^{13}C NMR data (Table 2 and Table S4) and the *m*/*z* of 490.0773 (HRESIMS, $[M + H]^+$). The formula indicated that the structure had 7 additional carbons, compared to **1**–**3**, suggesting a significant difference from the discorhabdin backbone. The primary difference in the ^1H NMR spectra was the presence of two 2H aromatic protons at δ_H 8.37 (d, H_2-24) and δ_H 7.56 (t, H_2-25), suggesting that the structure had a phenyl ring. This was confirmed using 2D NMR data that showed COSY correlation between the two, while H-25 had further COSY correlation to a 1H olefinic proton signal at δ_H 7.63 (H-26). Phenyl rings are unknown from previously described discorhabdin derivatives. Furthermore, H-25 had HMBC correlation to C-23 (δ_C 138.9) and H-24 had HMBC correlation to the deshielded C-22 (δ_C 189.1), suggesting a benzoyl substituent.

Other than that benzoyl group, the NMR data suggested a discorhabdin backbone with the presence of the C-6 spiro-center (δ_C 38.7), the C-3 oxymethine (δ_C 68.0) (C-3), and the C-11 deshielded quaternary carbon (δ_C 169.2). The 1D and 2D NMR data showed the backbone of **4** to have significant similarities to **1** with the only changes being two methylene groups in the place of the Δ^7-olefin, the C-7 bromine, and the loss of the proton previously seen on C-14. To complete the planar structure of **4**, the benzoyl substituent provides a ketone bridge between the phenyl ring and the open valence on C-14. While no correlations from H-16 to C-22 or H-24 to C-14 were present in multiple HMBC or LR-HMBC experiments, the open valence on C-14 offers the only plausible location for the benzoyl group.

Table 2. ^{1}H and ^{13}C NMR data for Discorhabdophenone A, B, and C (**4–6**) ((600 (^{1}H) and 150 (^{13}C) MHz, $(CD_3)_2SO$)).

Pos.	4		5		6	
	δ_C, Type	δ_H (*J* in Hz)	δ_C, Type	δ_H (*J* in Hz)	δ_C, Type	δ_H (*J* in Hz)
1	137.3, CH		67.2, CH	4.84, s	67.2, CH	4.85, t (1.8)
2	132.8, C		65.7, CH	5.02, s	65.7, CH	5.04, d (2.4)
3	68.0, CH	4.59, br s	184.5, C		184.5, C	
4a	29.6, CH_2	2.06, o/l	109.9, CH	5.96, s	110.0, CH	5.97, s
4b		1.90, o/l				
5	31.1, CH_2	2.10, o/l	171.3, CH		171.2, C	
		1.90, o/l				
6	38.7, C		47.5, C		47.5, C	
7a	31.1, CH_2	2.06, o/l	36.0, CH_2	2.86, d (10.9)	36.0, CH_2	2.86, dd (3.6, 10.7)
7b		1.63, td (3.1, 12.6)		2.61, d (11.2)		2.61, d (11.8)
8a	37.5, CH_2	3.55, dt (3.1, 13.3)	63.4, CH	5.70, s	63.4, CH	5.71, d (2.0)
8b		3.32, o/l				
9				9.30, s		9.34, s
10	145.6, C		145.5, C		145.2, C	
11	169.2, C		168.7, C		169.1, C	
12	133.2, C		132.3, C		133.2, C	
14	151.0, C		130.8, C		130.7, C	
15	122.1, C		121.1, C		121.3, C	
16	112.0, CH	7.84, d (5.7)	115.1, CH_2	7.94, (6.5)	114.9, CH	7.97, d (6.7)
17	129.9, CH	7.91, d (5.7)	131.5, CH_2	8.05, (6.4)	131.9, CH	8.10, d (6.5)
18						
19	139.2, C		146.0, C		145.4, C	
20	101.2, C		102.2, C		102.4, C	
21	132.1, C		132.7, C		132.5, C	
22	189.1, C		186.2, C		188.2, C	
23	138.9, C		129.2, C		138.0, C	
24	130.8, CH	8.37, d (5.6)	133.1, CH	8.42, d (8.2)	130.4, CH	8.35, d (7.8)
25	128.4, CH	7.56, t (7.5)	114.8, CH	6.90, d (8.2)	128.0, CH	7.55, t (7.6)
26	132.3, CH	7.63, t (6.9)	161.5, C		132.1, CH	7.63, t (7.4)

The *Latrunculia* sp. specimen from Palmer Station yielded two pyrroloiminoquinones with significant similarities to each other. One, discorhabdophenone B (**5**) displayed two 2H olefin doublets (H_2-24, δ_H 8.42; H_2-25, δ_H 6.90) compared to the second, discorhabdophenone C (**6**), with one olefinic doublet (H_2-24, δ_H 8.35) and two olefinic triplets (H_2-25, δ_H 7.55; H-26, δ_H 7.63). These shifts suggested that **5** had a *p*-disubstituted phenyl ring and that **6** had a mono-substituted phenyl ring, as found in **4**.

Discorhabdophenone B (**5**) was isolated with a *m*/*z* of 470.0810 (HRESIMS, $[M + H]^+$) and a molecular formula of $C_{25}H_{15}N_3O_4S$, corroborated by the ^{1}H and ^{13}C NMR data (Table 2). Structure elucidation was completed by COSY and HMBC correlations (Figure 3) and comparison with known discorhabdin derivatives. The compound was identified as a discorhabdin due to the C-6 spiro-center (δ_H 47.5) and the C-11 carbonyl (δ_C 168.7). The ^{1}H NMR data indicated that **5** had a *p*-substituted phenyl ring, two additional aromatic protons, four deshielded methines, and one methylene.

Discorhabdophenone B (**5**) differed from the previously presented discorhabdins herein due to the presence of a sulphur atom in the molecular formula; however, a C-5/C-8 sulphur bridge is a common feature among discorhabdin derivatives. Additional differences were the presence of three deshielded methines and the absence of the bromine atom, identified by the lack of a 1:1 isotopic pattern in the mass spectrum (Figure S36), and the presence of two extra deshielded quaternary carbons. The two deshielded methines H-1

(δ_H 4.84) and H-2 (δ_H 5.02) had COSY correlation to each other, with H-1 being identified as an oxymethine due to COSY correlation between the exchangeable δ_H 6.75 (OH-1) and H-1. H-2 displayed HMBC correlations to deshielded C-1 (δ_C 67.2), C-3 (δ_C 184.5), C-6 (δ_C 47.5), and C-17 (δ_C 131.5). H-4 (δ_H 5.96) had HMBC correlations to C-2 (δ_C 65.7), C-5 (δ_C 171.3), and C-6, identifying ring E, as shown in Figure 3, with a ketone on C-3, Δ^4 olefin, and an open valence on C-2 and C-5.

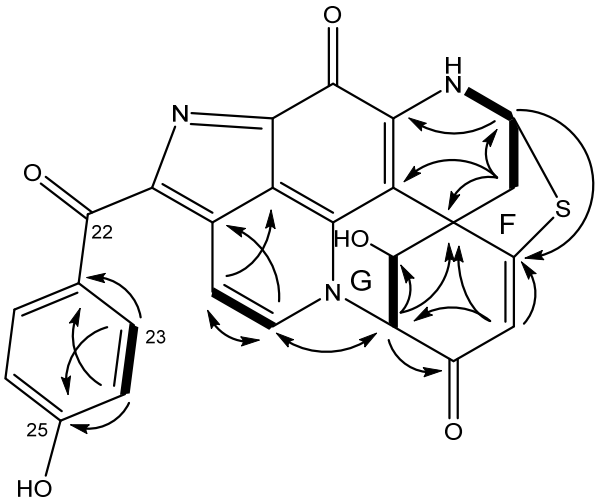

Figure 3. COSY (bold) and HMBC (arrow) correlations of **5** establishing new rings F and G.

The lack of a clear HMBC correlation from H_2-7 to C-1 left a level of uncertainty regarding the position of the carbonyl and hydroxy group on ring D. The chemical shift in the carbonyl suggested that it was part of a conjugated system, positioning it on C-3. Conversely, TOCSY correlations displayed evidence of a spin-coupled system between H-1/H-2/H-4, supporting the assignment of the hydroxy group to C-3. To determine the location of the carbonyl, DFT-based chemical shift predictions for the regioisomers of **5** were compared to the experimental chemical shift. The predicted chemical shifts in both thiol–ene and carbonyl carbons were in significantly better agreement with the experimental chemical shifts with the hydroxy group on C-1 and the carbonyl on C-3 (Figure 4A). Examination of the geometry-optimized conformer of **5** showed that H-2 and H-4 occupy the same plane (<10°). This is consistent with W-coupling between H-2/H-4, explaining the observed H-1/H-2/H-4 TOCSY spin system, while no direct COSY correlation from the hydroxyl (H-1) to H-4 was observed (Figure 4B).

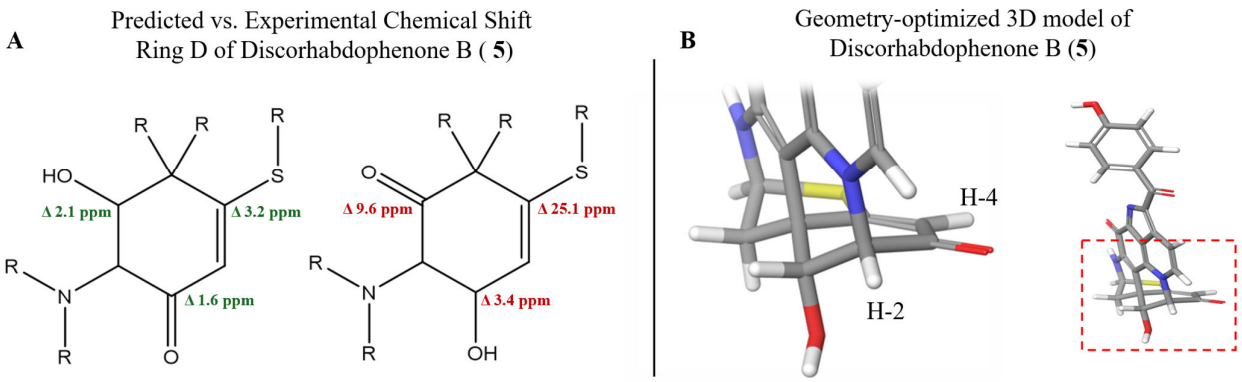

Figure 4. (**A**) Predicted vs. experimental chemical shifts in possible regioisomers of discorhabdophenone B (**5**) measured in delta ppm. (**B**) 3D model of geometry-optimized conformer of discorhabdophenone B (**5**) showing H-2 and H-4 are in the same plane of ring D.

The third deshielded methine H-8 (δ_H 5.70) displayed COSY correlations with methylene H_2-7 (δ_H 2.86/2.61) and the exchangeable H-9 (δ_H 9.30). Furthermore, H_2-7 showed HMBC correlations to C-6, C-8 (δ_C 63.4), and C-20, placing these in ring D. The open valences on C-5 and C-8 suggested the sulphur bridge previously mentioned. This was corroborated by HMBC correlations from H-8 to C-5. The two olefinic protons δ_H 7.94 (H-16) and δ_H 8.05 (H-17) were left to assign, with COSY correlations shown between the two and HMBC correlations from H-16 to C-19 (δ_C 146.0). H-17 had HMBC correlation to C-2, suggesting an N-18 to C-2 heterocycle, as reported for previous discorhabdin derivatives. Lastly, the previously established benzoyl group was connected to the discorhabdin backbone at the only remaining open valence, C-14, as observed in **4**.

Discorhabdophenone C (**6**) was isolated with the *m*/*z* of 454.0861 (HRESIMS, $[M + H]^+$). Corroborating ^{1}H and ^{13}C NMR data (Table 2), **6** was found with the molecular formula of $C_{25}H_{15}N_3O_4S$, which is one oxygen atom fewer than found in **5**. The 1D and 2D NMR data indicated a significant difference for C-26 (δ_C 161.5 for **5** and 132.1 for **6**), suggesting that **6** lacked the phenol function and congruent with the ^{1}H NMR analysis of the two that was described above. Unlike the reported discorhabdins which contain the C-2 to N-18 bridge, compounds **5** and **6** were not isolated in a protonated state. This was determined based on the number of exchangeable protons visible in ^{1}H NMR spectra, and the presence of sodium adducts $[M + Na]^+$ (**5**: calculated *m*/*z*: 492.0635, observed *m*/*z*: 492.0613, Δ 4.6 ppm; **6**: calculated *m*/*z*: 476.0681, observed *m*/*z*: 476.0679, Δ 0.4 ppm) in HRESIMS data (Figures S37 and S49) [9–11].

2.2. Stereochemical Analysis

2.2.1. Relative Stereochemistry

The stereochemistry of the new discorhabdin derivatives reported herein (**1**, **2** and **4–6**) was established based on coupling constants and chemical shift predictions using Density Functional Theory (DFT) and Gauge-Including Atomic Orbitals (GIAO). Compounds **1**, **2**, and **4** have two stereocenters, the C-6 spiro-center, which was prominent for all metabolites with the discorhabdins backbone, and a C-3 hydroxyl. As 2D Nuclear Overhauser Effect Spectroscopy (NOESY) correlations for **1**, **2**, and **4** from H-3 to methylene signals H-5 were inconclusive for determining relative configurations of C-3, DFT/GIAO-based chemical shift prediction and comparison tools DP4+ and Sorted Training Set (STS) were employed. A comparison of predicted ^{13}C shielding tensors for 3*S**,6*S** and 3*S**,6*R** for **1**, **2**, and **4**, at a B3LYP-D_3BJ/TZVP//wB97X-D3/6-31G* level, were compared to the experimental chemical shifts using STS, resulting in a 97%, 100%, and 100% probability of 3*S**,6*S** relative configuration for **1**, **2**, and **4**, respectively [12]. To increase our confidence in the assigned relative configuration, shielding tenors were additionally predicted at a B3LYP-D_3BJ/TZVP//B3YLP/6-311+G** level and compared using DP4+, yielding a 94%, 100%, and 100% probability of the three metabolites possessing a 3*S**,6*S** configuration when incorporating both ^{1}H and ^{13}C shielding tensors (Figure 5A) [13].

Compounds **5** and **6** have four chiral centers, C-1, C-2, C-6, and C-8, with eight theoretical relative configurations. Analysis of bond angles C-5/C-6/C-20 and C-1/C-6/C-7 of energy-minimized 3D models indicates that only 6*R**,8*S** or 6*S**,8*R** configurations possess plausible geometries around C-6, when C-5 and H-8 are on opposite faces of ring E, due to conformational constraints. Similarly, the examination of bond angles of 3D models, centering on C-2, limit H-2 and C-4 to occupying opposite faces of ring G, consistent with 1X, 2*S**,6*R**,8*S** (*X* = *R* or *S*) configurations (Figure 5A).

Examination of coupling constants between H-1/H-2 was inconclusive for the assignment of C-1 relative configuration, with $^3J_{HH}$ 2.4 Hz being consistent with a 64° dihedral angle, compared to 45° found for 1*R**, 2*R** and 82° found for 1*S**, 2*R**, respectively. To

determine the relative configuration of C-1, a comparison of DFT/GAIO-based chemical shift predictions and experimental was conducted for 1*R**,2*S**,6*R**,8*S** and 1*S**,2*S**,6*R**,8*S**, using the same methodology that was applied for **1**, **2**, and **4**. STS and the DP4+ probability calculator predicted >99% and 100% of 1*R**,2*S**,6*R**,8*S** relative configurations for both **5** and **6,** respectively (Figure 6B).

A

Predicted vs. Experimental Chemical Shifts

Compound	Relative configuration	DP4+			Sorted Training Set			
		B3LYP-D_3BJ/TZVP//B3YLP/6-311+G**			B3LYP-D_3BJ/TZVP//wB97X-D_3/6-31G*			
		^{1}H	^{13}C	All	$P_{Relative}$	P_{mean} (Significant >5%)	MAE	RMS
Discorhabdin G2 (**1**)	3*S**,6*R**	14.64%	26.25%	5.75%	2.94%	15.77%	1.97	2.60
	3*S,6*S****	**85.36%**	**73.75%**	**94.25%**	**97.06%**	**19.15%**	**1.84**	**2.36**
Discorhabdin G3 (**2**)	3*S**,6*R**	**100%**	0%	0%	0.00%	0.18%	4.24	3.40
	3*S,6*S****	0%	**100%**	**100%**	**100%**	**1.43%**	**5.91**	**4.73**
Discorhabdophenone A (**4**)	3*S**,6*R**	**96.27%**	0%	0%	0.00%	0.06%	4.57	6.62
	3*S,6*S****	3.73%	**100%**	**100%**	**100%**	**0.15%**	**4.26**	**6.20**

B

Predicted vs. Observed ECD spectra

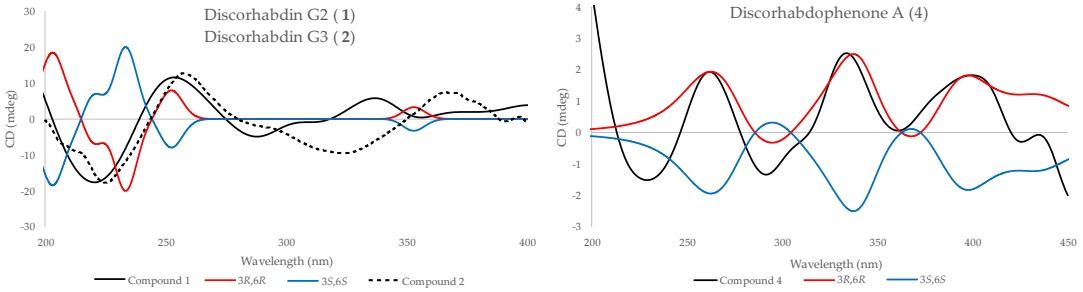

Figure 5. (**A**) DP4+ and STS probabilities from comparing experimental and DFT-predicted chemical shift in relative configurations of compounds **1**, **2**, and **4**, with results indicating 3*S**,6*S** configuration. (**B**) Experimental vs. observed ECD spectra of **1**, **2**, and **4**. Spectra were predicted and measured in methanol.

Geometry Optimized 3D Models of Discorhabdophenone C (6)

A

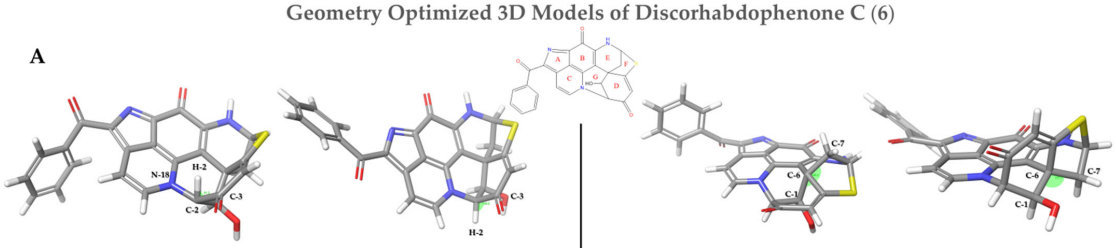

B

Predicted Vs Experimental Chemical Shifts

Compound	Relative configuration	DP4+			Sorted Training Set			
		B3LYP-D_3BJ/TZVP//B3YLP/6-311+G**			B3LYP-D_3BJ/TZVP//wB97X-D3/6-31G*			
		^{1}H	^{13}C	All	$P_{Relative}$	P_{mean} (Significant >5%)	MAE	RMS
Discorhabdophenone B (**5**)	**1R*,2S*, 6R*,8S***	**73.24%**	**100%**	**100%**	**99.84%**	**1.18%**	**3.16**	**5.21**
	1S*,2S*, 6R*,8S*	26.76%	0%	0%	0.16%	0.89%	3.35	5.32
Discorhabdophenone C (**6**)	**1R*,2S*, 6R*,8S***	36.79%	**100%**	**100%**	**99.9%**	**1.90%**	**2.98**	**4.91**
	1S*,2S*, 6R*,8S*	63.21%	0%	0%	0.09%	1.40%	3.22	5.03

Figure 6. (**A**) Geometry-optimized models of possible relative configurations of **6**, used to determine the bond angles and feasibility of relative configurations. (**B**) DP4+ and STS probabilities from comparing experimental and DFT-predicted chemical shift in relative configurations of compounds **5** and **6**, with results indicating a 1*R**,2*S**,6*R**,8*S** configuration.

2.2.2. Absolute Stereochemistry

The absolute configuration of compounds **1**, **2**, and **4**–**6** was determined by a comparison of experimental Electronic Circular Dichroism (ECD) and simulated ECD spectra using time-dependent density functional theory (TD-DFT), predicted at a B3LYP-D_3/CC-PVDZ// B3LYP-D_3/CC-PVDZ level using a PCM solvation model. Compounds **5** and **6** were assigned an absolute configuration of 1*S*,2*R*,6*S*,8*R* (Figure 7), while **1**, **2**, and **4** were assigned 3*R*,6*R* (Figure 5B). It is worth noting that the predicted spectra of **1** and **2** required a scaling factor of 0.65 to accurately match the experimental ECD spectra.

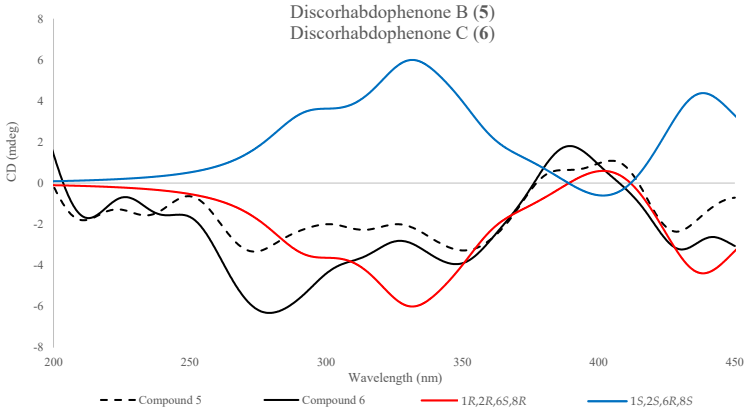

Figure 7. Comparison of observed ECD spectra of discorhabdophenone B (**5**, dashed-black) and discorhabdophenone C (**6**, solid-black) to the TD-DFT-predicted spectra of both epimers of **6**, 1*R*,2*S*,6*R*,8*S* (blue) and 1*S*,2*R*,6*S*,8*R* (red). Spectra were predicted and measured in methanol.

2.3. Bioactivity

The three crude extracts from specimens of *Latrunculia* spp. showed strong cytotoxic properties against a strain of human lung cells (A549) but no activity against *Candida albicans* nor *C. auras*. Upon the purification of metabolites, each were screened for their cytotoxic properties. The new discorhabdin derivatives **1** and **2** showed strong cytotoxicity, with IC_{50}'s (Table 3) of 4.3 µM and 1.8 µM, respectively, and the known metabolite (+)-debromodiscorhabdin A (**3**) showed an IC_{50} of 1.0 µM. No biological activity has been previously reported for (+)-debromodiscorhabdin A. Weak cytotoxicity was shown for **4**, with an IC_{50} of 23.9 µM (Table 3), while **5** and **6** were inactive in the cytotoxicity assay. Their activity profile suggested that the discorhabdin backbone had a strong influence on cytotoxicity, with a decrease in cytotoxicity for **4** which had a Δ^{16} olefin compared to the Δ^{7} olefins shown for **1** and **2**. Additionally, **4** had a benzophenone substituent. The benzophenone substituent was also present in **5** and **6** but neither showed cytotoxicity when tested at 50 µg/mL. Compounds **5** and **6** differed from **4** in terms of the C-2/N-18 bridge, a C-5/C-8 sulphur bridge, and $\Delta^{4,16}$ olefins. Such structural insights may shed light on a cytotoxicity-optimized derivative.

Table 3. Cytotoxicity activity against the A549 cells (IC_{50}).

Compound	IC_{50} (µM)	SD [a] (µM)
1	4.3	1.1
2	1.8	0.1
3	1.0	0.4
4	23.9	0.3
5	>50	ND [b]
6	>50	ND [b]

a = standard deviation; b = not determined.

3. Materials and Methods

3.1. General Experimental Procedures

Optical rotations were measured using an AutoPol IV digital polarimeter (Hackettstown, NJ, USA) at 589 nm with a 1 dm path length cell. UV-Vis spectra were extracted from HPLC chromatograms. NMR spectra were acquired using a Bruker Neo 600 MHz broadband spectrophotometer (Rheinstetten, Germany). The residual solvent peaks were used as an internal chemical shift reference ($(CD_3)_2SO$: δ_C 39.5; δ_H 2.50). High-resolution mass spectrometry–liquid chromatography data were obtained on an Agilent 6540 LC-MS QTOF (Wilmington, DE, USA) coupled to an Agilent Jet-stream electrospray ionization detector. H_2O + 0.1% FA (A) and CH_3CN + 0.1% FA (B) were used as mobile phases on a Phenomenex Kinetex C_{18} column (2.6 µm, 100 Å, 150 × 3 mm: 0.5 mL/min) (Torrance, CA, USA). Reverse-phase HPLC was performed on a Shimadzu LC20-AT system (Canby, OR, USA) equipped with a photodiode array detector (M20A) using a preparative Phenomenex C_{18} column (5 µm, 100 Å, 250 × 21.2 mm: 10 mL/min) or a semi-preparative Phenomenex C_{18} column (10 µm, 100 Å, 250 × 10 mm: 4 mL/min). CCS values were measured on an Agilent 6560c LC-IMS-Q-TOF (Wilmington, DE, USA) using high-purity N_2, with CCS values referenced to Agilent ESI tune Mix, in positive mode, with CCS value calculations using Agilent Mass Hunter IM-MS Browser (build 10.0.1.10039). The drift gas temperature was 27 °C at 3.940 torr. The electronic field was 18.549 V/cm. The methanol and acetonitrile used for column chromatography were obtained from Fisher Co. (Waltham, MA, USA) and were HPLC grade (>99% purity), while the H_2O was distilled and filtered. Solvents mixtures are reported as % *v*/*v*.

3.2. Biological Materials

Two specimens of *Latrunculia* cf. *biformis* (Figure S50) were collected at 210 m depth from the Kerguelen Plateau, Antarctica (−51.137 S, 71.8269 E), by trawling (sample codes ACE16-49, WAMZ44145; ACE16-51, WAMZ44147), with wet weights of 0.15 kg and 1.5 kg, respectively. An additional specimen (sample code PSC18-41, wet weight: 3.3 kg) of *Latrunculia* sp. (Figure S50) was collected by SCUBA at 40 m depth from Cormorant Island near Palmer station, Antarctica (−64.77551 S; −64.071805 W). A small piece of tissue from the two specimens from the Kerguelen Plateau were extracted for DNA using the Qiagen Blood & Tissue DNeasy kit according to the manufacturer's instructions. A fragment of the mitochondrial Cytochrome Oxidase I (COI) gene was amplified by PCR using primers from [14], purified enzymatically, and bidirectionally Sanger sequenced at the Australian Genome Research Facility (AGRF, Perth, Australia). Reads were assembled and edited using Geneious Prime v2022.1, and analyzed with other relevant data from NCBI in a Maximum Likelihood framework in IQ-tree [15] implementing ModelFinder [16]. The resulting tree shows the phylogenetic placement of the specimens (Figure S51).

3.3. Extraction, Isolation, and Purification

Specimens were kept frozen upon collection and freeze-dried on return to our lab. Upon analysis, the three freeze-dried specimens were crushed and extracted separately in MeOH for 24 h. The extracts were filtered and replaced with fresh MeOH twice. Extracts from the three specimens were separately eluted from the HP20 by first washing the fresh resin with Me_2CO before pre-equilibrating the columns with H_2O. The extracts were then applied to the resin and eluted from their respective HP20 column before the eluent was diluted with equal volume H_2O and again eluted from the column. This was repeated a second time. Three fractions of decreasing polarity were created by eluting the column with (A) 30% Me_2CO/H_2O, (B) 75% Me_2CO/H_2O, and (C) 100% Me_2CO. Fraction B was further pursued for all three specimens.

Preparative C_{18} HPLC was performed on ACE16-49B (420 mg) with a gradient of 50–100% ACN/H_2O over 30 min, resulting in 12 fractions, designated B1–B12. The mass spectrum (MS) indicated that fractions B1 (32.4 mg) and B6 (50.2 mg) contained brominated metabolites and therefore they were further prioritized. Fraction B1 was further fractionated by semipreparative C_{18} HPLC with a 10–100% MeOH/H_2O gradient over 30 min, resulting in the pure compound B1-B. B1-B (**2**: 10 mg, RT = 13.7 min) and B6 (**1**: 50.2 mg, RT = 23.4 min) were determined pure compounds by ^{1}H NMR spectroscopy. ACE16-51B (8.3 g) and PSC18-41B (6.2 g) were purified by RP-MPLC with a gradient of 10–100% MeOH/H_2O over 60 min, resulting in 12 fractions each, designated as B1-B12. Fractions B2, B7, and B8 from ACE16-51 were further fractionated by semipreparative C_{18} HPLC with a gradient of 30–100% ACN/H_2O (0.1% FA), resulting in the pure compounds (+)-debromodiscorhabdin A (**3**: 2.4'mg, RT = 12.1 min) and discorhabdophenone A (**4**: 6.3 mg, RT = 16.5 min), determined pure by ^{1}H NMR spectroscopy. MPLC fractions B6, B7, and B8 from PSC18-41 were all combined due to similarities in ^{1}H NMR and MS spectra. They were fractionated by semipreparative C_{18} HPLC with a gradient of 20–100% ACN/H_2O (0.1% FA) over 30 min, resulting in the pure compounds discorhabdophenone B (**5**: 4.5 mg, RT = 7 min) and discorhabdophenone C (**6**: 1.9 mg, RT = 18.2 min).

*3.4. Spectroscopic Data (**1**, **2**, and **4**–**6**)*

Discorhabdin G2 (**1**): deep-red solid; $[\alpha]_D^{22}$ −241.4 (*c* 0.029, MeOH); UV (MeOH/H_2O) λ_{max} (log ε) 211, 228 (sh), 463 (sh) nm (8.22, 8.53, 1.65); ^{1}H NMR (600 MHz) and ^{13}C NMR (150 MHz) data, see Table 1 and Table S1; HRESIMS *m*/*z* 463.9450 $[M + H]^+$ (calcd for $C_{18}H_{14}O_2N_3{}^{79}Br$, 463.9427; Δ 4.96 ppm). CCS $[M + H]^+$ 195.8 Å2.

Discorhabdin G3 (**2**): green solid; $[\alpha]_D^{22}$ +207.4 (*c* 0.068, MeOH); UV (MeOH/H_2O λ_{max} (log ε) 207, 247 (sh), 336 (sh), 564 (sh) nm (7.45, 5.99, 2.79, 0.34); ^{1}H NMR (400 MHz) and ^{13}C NMR (100 MHz) data, see Table 1 and Table S2; HRESIMS *m*/*z* 386.0505 $[M + H]^+$ (calcd for $C_{18}H_{17}O_2N_3{}^{79}Br_2$, 386.0499; Δ 1.6 ppm). CCS $[M + H]^+$ 193.0 Å2.

(+)-Debromodiscorhabdin A (**3**) was dereplicated by Small Molecular Accurate Recognition Technology (SMART) NMR, with a cosine score of 0.890, by the use of its HSQC data [17]. Compound **3** was identified by its multiplicity-edited HSQC data as having three olefinic protons, two deshielded methines, and four methylene groups. Its HRESIMS displayed an $[M + H]^+$ ion at *m*/*z* 338.0976, which, with its ^{1}H and ^{13}C NMR data (see Table S3), matches the molecular formula of $C_{18}H_{16}N_3O_2S$ for the known debromodiscorhabdin A (**3**) [7]. The published optical rotation of $[\alpha]_D^{22}$ +207 agrees well the experimental optical rotation of $[\alpha]_D^{22}$ +178.9.

Discorhabdophenone A (**4**): deep-red solid; $[\alpha]_D^{22}$ +66.0 (*c* 0.076, MeOH); UV (ACN/H_2O) λ_{max} (log ε) 229, 306 (sh), 462 (sh) nm (21.96, 11.67, 4.03); ^{1}H NMR (400 MHz) and ^{13}C NMR (100 MHz) data, see Table 2 and Table S4; HRESIMS *m*/*z* 490.0773 $[M + H]^+$ (calcd for $C_{25}H_{21}O_3N_3{}^{79}Br$, 490.0761; Δ 2.5 ppm). CCS $[M + H]^+$ 214.1 Å2.

Discorhabdophenone B (**5**): deep-red solid; $[\alpha]_D^{22}$ +310.5 (*c* 0.11, MeOH); UV (ACN/H_2O) λ_{max} (log ε) 214, 282 (sh), 469 (sh) nm (19.16, 14.65, 3.68); ^{1}H NMR (400 MHz) and ^{13}C NMR (100 MHz) data, see Table 2 and Table S5; HRESIMS *m*/*z* 470.0810 $[M + H]^+$ (calcd for $C_{25}H_{16}O_5N_3S$, 470.0805; Δ 1.1 ppm). CCS $[M + H]^+$ 208.2 Å2.

Discorhabdophenone C (**6**): deep-red solid; $[\alpha]_D^{22}$ +229.2 (*c* 0.096, MeOH); UV (ACN/H_2O) λ_{max} (log ε) 205, 282 (sh), 475 (sh) nm (10.11, 6.76, 1.97); ^{1}H NMR (400 MHz) and ^{13}C NMR (100 MHz) data, see Table 2 and Table S6; HRESIMS *m*/*z* 454.0861 $[M + H]^+$ (calcd for $C_{25}H_{16}O_4N_3S$, 454.0856; Δ 1.1 ppm). CCS $[M + H]^+$ 208.1 Å2.

3.5. Computational Methods

All molecular mechanics and quantum mechanics calculations were integrated using Macromodel and Jaguar (version 2024-1, Schrodinger LLC) and ORCA 6.0.1 [18–23].

3.5.1. Conformer Generation

Conformation searches for each isomer utilized OPLS4 to generate low-energy conformers within a 5 kcal/mol energy window, in the liquid phase (water), using a mixed torsional/low-mode sampling approach. Conformers with <0.5 Å atom deviation were removed to prevent redundancy.

3.5.2. Chemical Shift and Shielding Tensor Predictions

Conformers underwent geometry optimization using DFT at the B3LYP-D3(BJ)/TZVP level with a CPCM (DMSO) solvation model and tightSCF convergence tolerance using ORCA 6.0.1. Frequency calculations were conducted on geometry-optimized conformers and conformers with a negative frequency were re-optimized with an extremeSCF convergence tolerance. NMR shielding tensors were predicted using DFT/GIAO at the ωB97X-D/6-31G* level, with bromine atoms being calculated at the ωB97X-D/6-311G* level, using a CPCM solvation model (DMSO), for use with the Sorted Training Set (STS) comparison tool. Shielding tensor predictions were repeated at a B3YLP/6-311+G** level for use with the DP4+ probability predictor. Boltzmann-weighted shielding tensors were calculated based on each conformers Gibbs Free energy calculated at B3LYP-D3(BJ)/TZVP level. A Sorted Training Set (STS) excel sheet was used to compare the experimental ^{13}C chemical shift to predicted chemical shifts for each configuration. Additionally, a DP4+ excel sheet was used for a comparison of experimental ^{1}H and ^{13}C chemical shifts to predicted shielding tensors. The experimental and predicted chemical shifts in the non-equivalent protons were aligned based on their relative shielding, with upfield and downfield trends used to guide the assignments. Exchangeable protons were excluded from chemical shift comparisons. Metabolites were calculated as neutral molecules.

3.5.3. Electronic Circular Dichroism Spectral Predictions

Conformers underwent geometry optimization and subsequent relative thermal free energies (ΔG) at 298.15 K, using DFT at the B3LYP-D3/cc-pVDZ level. Geometry optimization was carried out using a methanol PCM solvation model, while single-point energy calculations were conducted using a PBF solvent model for improved energy calculation accuracy. Conformers with negative vibrational frequencies were removed. ECD spectra for each conformer were computed using TD-DFT at the B3LYP-D3/cc-pVDZ level, using 20 excited states generated by Tamm–Dancoff approximation. Boltzmann conformer populations were used to create a weighted averaged ECD spectrum. Experimental and predicted spectra were visualized using Excel and a Schrodinger spectral plot tool. A comparison between experimental and predicted UV spectra was used to determine wavelength corrections. Predicted ECD spectra were normalized to match the intensities of experimental signals. Metabolites were calculated as neutral molecules. The predicted spectra of **1** and **2** required a scaling factor of 0.65 to accurately match the experimental ECD spectra.

3.6. Cytotoxicity Assay

Stock solutions of A549 cells were prepared at 1×10^4 cells/mL in growth media (FK12 medium Kaighn's modification, 10% bovine growth serum, 1% penicillin-streptomycin) using a calibration curve based on UV-Vis absorbance at 450, 530, and 600 nm. To each well of a 96-well plate 200 µL of this solution was added and incubated for 24 h at 37 °C and 5% CO_2 atmosphere. Each testing solution (2 µL) was then added to the wells in triplicate

and the plate was incubated for 72 h, at which point the media in each plate was removed and each well was washed with 1× phosphate-buffered saline (PBS). After the solution of MTT (1.25 mg/mL in 75% growth media 25% PBS) was added to each well, the plate was incubated. After 4 h of incubation, the media was removed carefully to avoid disturbing the crystals in the bottom of each well. DMSO (200 µL) was added to each well and the cell viability was calculated as a percentage using the negative control. DMSO was used as a negative control, and the positive control was nystatin.

4. Conclusions

Three specimens of *Latrunculia* spp. from two different Southern Ocean locations were found with new discorhabdin derivatives, including the novel C-14 phenone function. The highly colored metabolites were purified using RP-HPLC by targeting characteristic ^{1}H NMR signals and masses that sometimes displayed isotopic patterns. Five unreported metabolites were isolated, **1**, **2,** and **5**–**6**, as well as one previously described metabolite, **3**. Their cytotoxic properties were investigated against the A549 cell lines, where **1** and **2** displayed significant cytotoxicity at 4.3 µM and 1.8 µM, respectively. Compounds **4**–**6** showed weak or no cytotoxicity and differ from the other discorhabdins by the aforementioned phenone substituent.

Supplementary Materials: The following supporting information can be downloaded at https://www.mdpi.com/article/10.3390/md23100401/s1. Figures S1–S51 and Tables S1–S6: ^{1}H, ^{13}C, COSY, HSQC, and HMBC NMR spectra, as well as HRMS, and geometry-optimized conformers of metabolites **1**, **2,** and **4**–**6**; maximum likelihood tree of Latrunculiidae COI; photographs of study specimens.

Author Contributions: Conceptualization, B.J.B. and N.G.W.; methodology, S.S.H.O., S.A., E.C.R. and B.J.B.; formal analysis, S.S.H.O., S.A. and E.C.R.; taxonomy, N.G.W. and B.J.B.; data curation, S.A., S.S.H.O., N.G.W. and B.J.B.; writing—original draft preparation, S.S.H.O. and S.A.; writing—review and editing, all authors; supervision, B.J.B.; funding acquisition, B.J.B. and N.G.W. All authors have read and agreed to the published version of the manuscript.

Funding: This work was supported by the US National Institutes of Health grant R21 AT010939 and R56 AI154922, National Science Foundation grant PLR-1341339 to B.J.B., and by the Antarctic Circumnavigation Expedition (carried out by the Swiss Polar Institute, supported by the ACE Foundation and Ferring Pharmaceuticals). A portion of this work was performed in the McKnight Brain Institute at the National High Magnetic Field Laboratory's Advanced Magnetic Resonance Imaging and Spectroscopy (AMRIS) Facility, which is supported by National Science Foundation Cooperative Agreement DMR-2128556 and the State of Florida.

Institutional Review Board Statement: Not applicable.

Data Availability Statement: The NMR data for the following compounds have been deposited in the Natural Products Magnetic Resonance Database (NP-MRD; www.np-mrd.org, accessed on 30 July 2025 and can be found at NP0351379 (Discorhabdin G2), NP0351380 (Discorhabdin G3), NP0351381 (Discorhabdophenone A), NP0351382 (Discorhabdophenone B), and NP NP0351383 (Discorhabdophenone C). Other data not found in the Supplementary Materials will be available upon request to the corresponding author.

Acknowledgments: The authors wish to thank the crew and science participants of the Antarctic Circumnavigation Expedition, and acknowledge collection permit 2016-168 for the French southern and Antarctic lands. We also thank USF core facility staff, including the Directors of the Chemical Purification, Analysis, and Screening, and the Interdisciplinary NMR Facility, and the collections staff at the Western Australian Museum, with particular thanks to Alex Hickling.

Conflicts of Interest: The authors declare no conflicts of interest.

References

1. Hu, J.-F.; Fan, H.; Xiong, J.; Wu, S.-B. Discorhabdins and pyrroloiminoquinone-related alkaloids. *Chem. Rev.* **2011**, *111*, 5465–5491. [CrossRef] [PubMed]
2. Kalinski, J.-C.J.; Polyzois, A.; Waterworth, S.C.; Siwe Noundou, X.; Dorrington, R.A. Current perspectives on pyrroloiminoquinones: Distribution, biosynthesis and drug discovery potential. *Molecules* **2022**, *27*, 8724. [CrossRef] [PubMed]
3. Na, M.; Ding, Y.; Wang, B.; Tekwani, B.L.; Schinazi, R.F.; Franzblau, S.; Kelly, M.; Stone, R.; Li, X.-C.; Ferreira, D.; et al. Anti-infective discorhabdins from a deep-water Alaskan sponge of the senus *Latrunculia*. *J. Nat. Prod.* **2010**, *73*, 383–387. [CrossRef] [PubMed]
4. Li, F.; Peifer, C.; Janussen, D.; Tasdemir, D. New discorhabdin alkaloids from the Antarctic deep-sea sponge *Latrunculia biformis*. *Mar. Drugs* **2019**, *17*, 439. [CrossRef]
5. Li, F.; Kelly, M.; Tasdemir, D. Chemistry, chemotaxonomy and biological activity of the Latrunculid sponges (Order Poecilosclerida, Family Latrunculiidae). *Mar. Drugs* **2021**, *19*, 27. [CrossRef]
6. Lang, G.; Pinkert, A.; Blunt, J.W.; Munro, M.H.G. Discorhabdin W, the first dimeric discorhabdin. *J. Nat. Prod.* **2005**, *68*, 1796–1798. [CrossRef]
7. El-Naggar, M.; Capon, R.J. Discorhabdins revisited: Cytotoxic alkaloids from Southern Australian marine sponges of the genera *Higginsia* and *Spongosorites*. *J. Nat. Prod.* **2009**, *72*, 460–464. [CrossRef]
8. Yang, A.; Baker, B.J.; Grimwade, J.; Leonard, A.; McClintock, J.B. Discorhabdin alkaloids from the Antarctic sponge *Latrunculia apicalis*. *J. Nat. Prod.* **1995**, *58*, 1596–1599. [CrossRef]
9. Grkovic, T.; Pearce, A.N.; Munro, M.H.G.; Blunt, J.W.; Davies-Coleman, M.T.; Copp, B.R. Isolation and characterization of diastereomers of discorhabdins H and K and assignment of absolute configuration to discorhabdins D, N, Q, S, T, and U. *J. Nat. Prod.* **2010**, *73*, 1686–1693. [CrossRef]
10. Grkovic, T.; Ding, Y.; Li, X.-C.; Webb, V.L.; Ferreira, D.; Copp, B.R. Enantiomeric discorhabdin alkaloids and establishment of their absolute configurations using theoretical calculations of electronic circular dichroism spectra. *J. Org. Chem.* **2008**, *73*, 9133–9136. [CrossRef]
11. Jeon, J.-E.; Na, Z.; Jung, M.; Lee, H.-S.; Sim, C.J.; Nahm, K.; Oh, K.-B.; Shin, J. Discorhabdins from the Korean marine sponge *Sceptrella* sp. *J. Nat. Prod.* **2010**, *73*, 258–262. [CrossRef]
12. Li, J.; Liu, J.-K.; Wang, W.-X. GIAO ^{13}C NMR calculation with sorted training sets improves accuracy and reliability for structural assignation. *J. Org. Chem.* **2020**, *85*, 11350–11358. [CrossRef] [PubMed]
13. Zanardi, M.M.; Sarotti, A.M. Sensitivity analysis of DP4+ with the probability distribution terms: Development of a universal and customizable method. *J. Org. Chem.* **2021**, *86*, 8544–8548. [CrossRef] [PubMed]
14. Geller, J.; Meyer, C.; Parker, M.; Hawk, H. Redesign of PCR primers for mitochondrial cytochrome c oxidase subunit I for marine invertebrates and application in all-taxa biotic surveys. *Mol. Ecol. Resour.* **2013**, *13*, 851–861. [CrossRef] [PubMed]
15. Trifinopoulos, J.; Nguyen, L.-T.; von Haeseler, A.; Minh, B.Q. W-IQ-TREE: A fast online phylogenetic tool for maximum likelihood analysis. *Nucleic Acids Res.* **2016**, *44*, W232–W235. [CrossRef]
16. Kalyaanamoorthy, S.; Minh, B.Q.; Wong, T.K.F.; von Haeseler, A.; Jermiin, L.S. ModelFinder: Fast model selection for accurate phylogenetic estimates. *Nat. Methods* **2017**, *14*, 587–589. [CrossRef]
17. Zhang, C.; Idelbayev, Y.; Roberts, N.; Tao, Y.; Nannapaneni, Y.; Duggan, B.M.; Min, J.; Lin, E.C.; Gerwick, E.C.; Cottrell, G.W.; et al. Small Molecule Accurate Recognition Technology (SMART) to enhance natural products research. *Sci. Rep.* **2017**, *7*, 14243. [CrossRef]
18. Izsák, R.; Neese, F. An overlap fitted chain of spheres exchange method. *J. Phys. Chem.* **2011**, *135*, 144105. [CrossRef]
19. Izsák, R.; Hansen, A.; Neese, F. The resolution of identity and chain of spheres approximations for the LPNO-CCSD singles Fock term. *Mol. Phys.* **2012**, *110*, 2413–2417. [CrossRef]
20. Neese, F. The ORCA program system. *WIREs Comput. Mol. Sci.* **2012**, *2*, 73–78. [CrossRef]
21. Izsák, R.; Neese, F.; Klopper, W. Robust fitting techniques in the chain of spheres approximation to the Fock exchange: The role of the complementary space. *J. Chem. Phys.* **2013**, *139*, 094111. [CrossRef]
22. Neese, F. Software update: The ORCA program system, version 4.0. *WIREs Comput. Mol. Sci.* **2018**, *8*, e1327. [CrossRef]
23. Neese, F.; Wennmohs, F.; Becker, U.; Riplinger, C. The ORCA quantum chemistry program package. *J. Chem. Phys.* **2020**, *152*, 224108. [CrossRef]